Lithology and orographic precipitation control river incision in the tropical Andes

Benjamin Campforts[a,b,*], Veerle Vanacker[c], Frédéric Herman[d], Matthias Vanmaercke[e], Wolfgang Schwanghart[f], Gustavo E. Tenorio[b,g], Patrick Willems[h], Gerard Govers[b]

[a] *Research Foundation Flanders (FWO), Egmontstraat 5, 1000 Brussels, Belgium*

[b] *Department of Earth and Environmental Sciences, KU Leuven, Celestijnenlaan 200E, 3001 Heverlee, Belgium*

[c] *Earth and Life Institute, Georges Lemaître Centre for Earth and Climate Research, University of Louvain, Place Louis Pasteur 3, 1348 Louvain-la-Neuve, Belgium*

[d] *Institute of Earth Surface Dynamics, University of Lausanne, CH-1015 Lausanne, Switzerland*

[e] *Université de Liège, Département de Géographie, Clos Mercator 3, 4000 Liège, Belgium*

[f] *Institute of Earth and Environmental Sciences, University of Potsdam, Germany*

[g] *Facultad de Ciencias Agropecuarias, Universidad de Cuenca, Campus Yanuncay, Cuenca, Ecuador*

[h] *Department of Civil Engineering – Hydraulics Section, KU Leuven, Kasteelpark 40 box 2448, 3001 Leuven, Belgium*

[*] *Corresponding author: Tel.: +32 16326426, E-mail: benjamin.campforts@kuleuven.be*

Contents of this file

Additional supporting information (uploaded as separated .xlsx files)

Text S1: Topographic analysis

To compare inter-catchment variability of river steepness indices, the referenced concavity index (θ) is typically fixed to a value of 0.45 (DiBiase et al., 2010). In this section we explore whether assuming a fixed value for the concavity index is consistent with the diversity of river forms in the Paute basin. Our analysis relies on Bayesian optimization of the *mn*-ratio as implemented in the TopoToolbox function mnoptim (see also https://topotoolbox.wordpress.com/2017/10/24/bayesian-optimization-of-the-mn-ratio/).

The Paute river network is characterized by a major transient knickzone, situated close to the outlet of the basin (see main text for discussion). Including this knickzone in the *mn*-analysis would render the concavity to be significantly lower due to a major jump in the slope area profiles (Figure S3). It is known that there exists a positive trade-off between the concavity and the steepness of river profiles in transient regions (Vanacker et al., 2015). In order to facilitate the use of the stochastic stream power equation and ensure inter catchment comparability, we fixed the concavity to a value representative for the part of the river network being close to equilibrium. Therefore, we only considered the streams upstream of the two major knickzones in the Paute network, both likely originating from a major river reorganization in the recent geological past (<10 Ma Steinmann et al., 1999).

The Bayesian optimization procedure is based on the integral approach of longitudinal river profile analysis (chi-analysis) (Perron and Royden, 2013). Moreover, the optimization uses a cross-validation approach which randomly and repeatedly separates the drainage network into training and validation data. In one iteration, the *mn* -ratio is determined with the training data (~50% of the catchments) and is then evaluated with the remaining data (validation data) using the root mean squared error (RMSE). This approach is stochastic because at each iteration, different catchments are randomly selected. The RMSE for the same value of the concavity index may thus differ, which enables us to quantify the uncertainty of the optimal concavity. Bayesian optimization returns an optimal value of the $\theta = 0.42$ and is consistent with the value of 0.45 which is commonly used when modelling stochastic river incision (DiBiase and Whipple, 2011; Scherler et al., 2017). Uncertainty analysis (Figure S3) reveals that a range of *mn*-values between 0.35 and 0.5 is likely to result in equal model performance, further justifying adopting θ to 0.45 for the remainder of this study.

Chi-plots of drainage network for all individual sub catchments studied in this paper are shown in Figure S4.

Figure S5 illustrates the location of the digitized river sections to calibrate the river discharge-width relationship (main manuscript, Figure 3).

Table S1 Lithological erodibility index (L_A) based on the age of the lithological unit

	L_A
Cambrium	1
Ordovicium	1.2
Silurian	1.3
Devonian	1.5
Carboniferous	1.8
Permian	2.5
Permian/Triassic	2.6
Triassic	2.7
Triassic/Jurassic	3
Jurassic	3.3
Jurassic/Cretaceous	3.7
Cretaceous	4.2
Cretaceous/Paleogene	4.6
Paleogene	5.2
Paleogene/Neogene	5.5
Neogene	5.8
Neogene/Quaternary	5.9
Quaternary	6

Table S2 Lithological erodibility index (L_L) per lithology, adjusted from on Aalto et al. (2006)

Igneous	L_L	**Metamorphic**	L_L	**Strong sedimentary**	L_L	**Unconsolidated**	L_L
Adamellite		Gneiss		Limestone		Alluvial deposits	
Diorite		Amphibolite		Massive greywacke	4	Colluvial deposits	
Dolerite		Chert	2	Massive mudstone		Estuarine deposits	12
Diabase		Migmatite		Massive sandstone		Marine deposits	
Gabbro		Serpentinite				Laterite	
Granite	2						
Granodiorite		**Metasedimentary**		**Weak sedimentary**			
Granophyre		Quartzite	2	Conglomerates			
Ophiolite		Meta lava	3	Pyroclastic	10		
Pegmatite		Schist	4	Shale			
Porphyry		Slate		Weathered sandstone			
Ultramafic				Loose volcanic deposits	12		
Andesite							
Basaltic Lava							
Rocks	3						
Ignimbrite							
Nepheline							

Table S3 Lithostratigraphic data

See file “TableS3.xlsx”

Table S4 Data PRECUPA

See file “TableS4.xlsx”

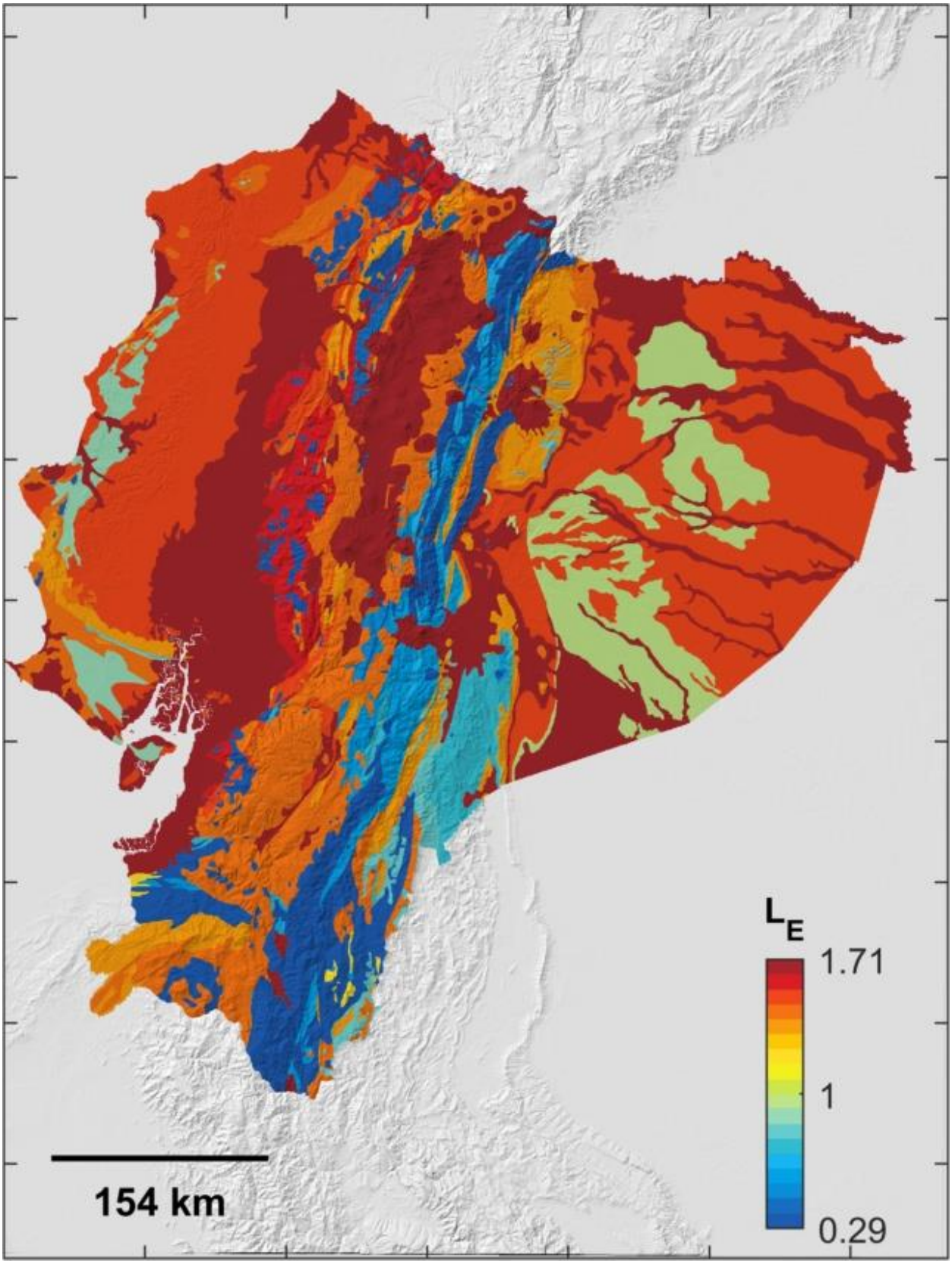

Figure S1 Regionally constrained lithological erodibility index (L_E) derived from the 1M geological map of Ecuador (Egüez et al., 2017) and applying Eq. 15, overlain on hillshade map based on the 30 m SRTM v3 DEM (NASA JPL, 2013).

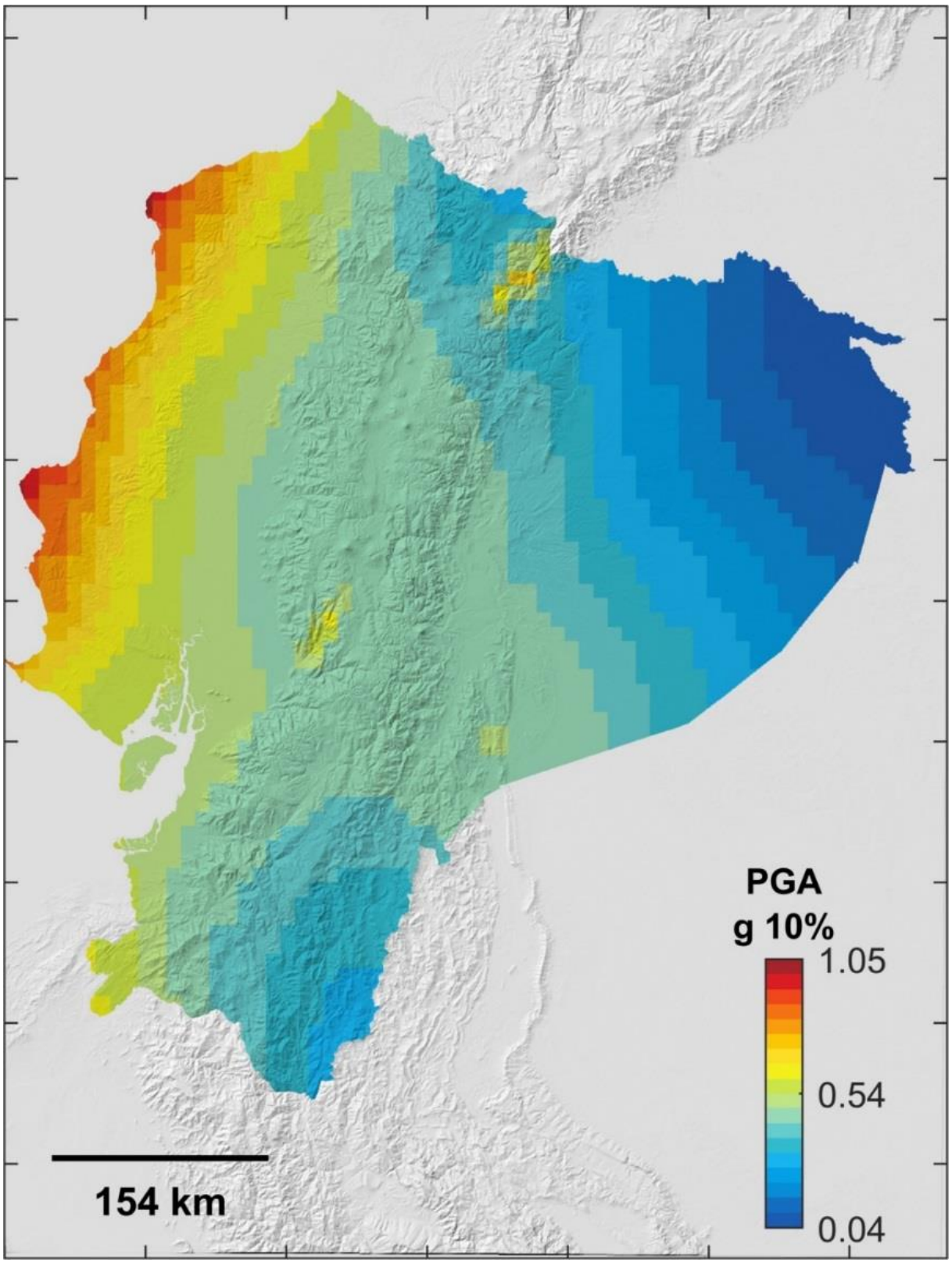

Figure S2 PGA (g) derived from Petersen et al. (2018) overlain on hillshade map based on the 30 m SRTM v3 DEM (NASA JPL, 2013). PGA data available through ScienceBase (doi: 10.5066/F7WM1BK1).

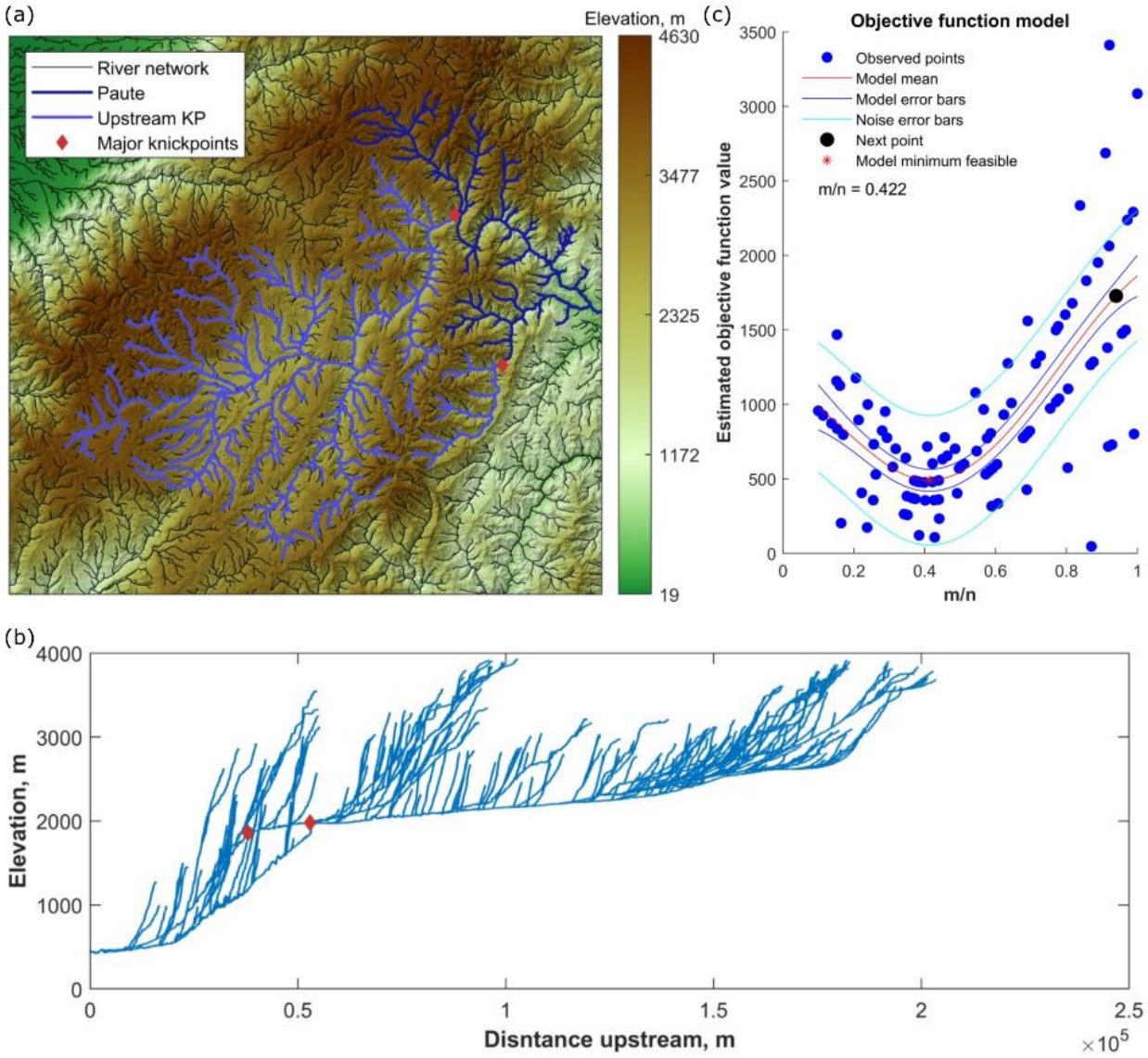

65

Figure S3: Constraining the concavity index of the Paute catchment using an objective function model. (a) River network with major knickpoints indicated as red diamonds, overlain on hillshade map based on the 30 m SRTM v3 DEM (NASA JPL, 2013), (b) Longitudinal river profiles of the Paute drainage network. (c) Bayesian optimization of *mn*-ratio for the stream network upstream of the two major knickzones.

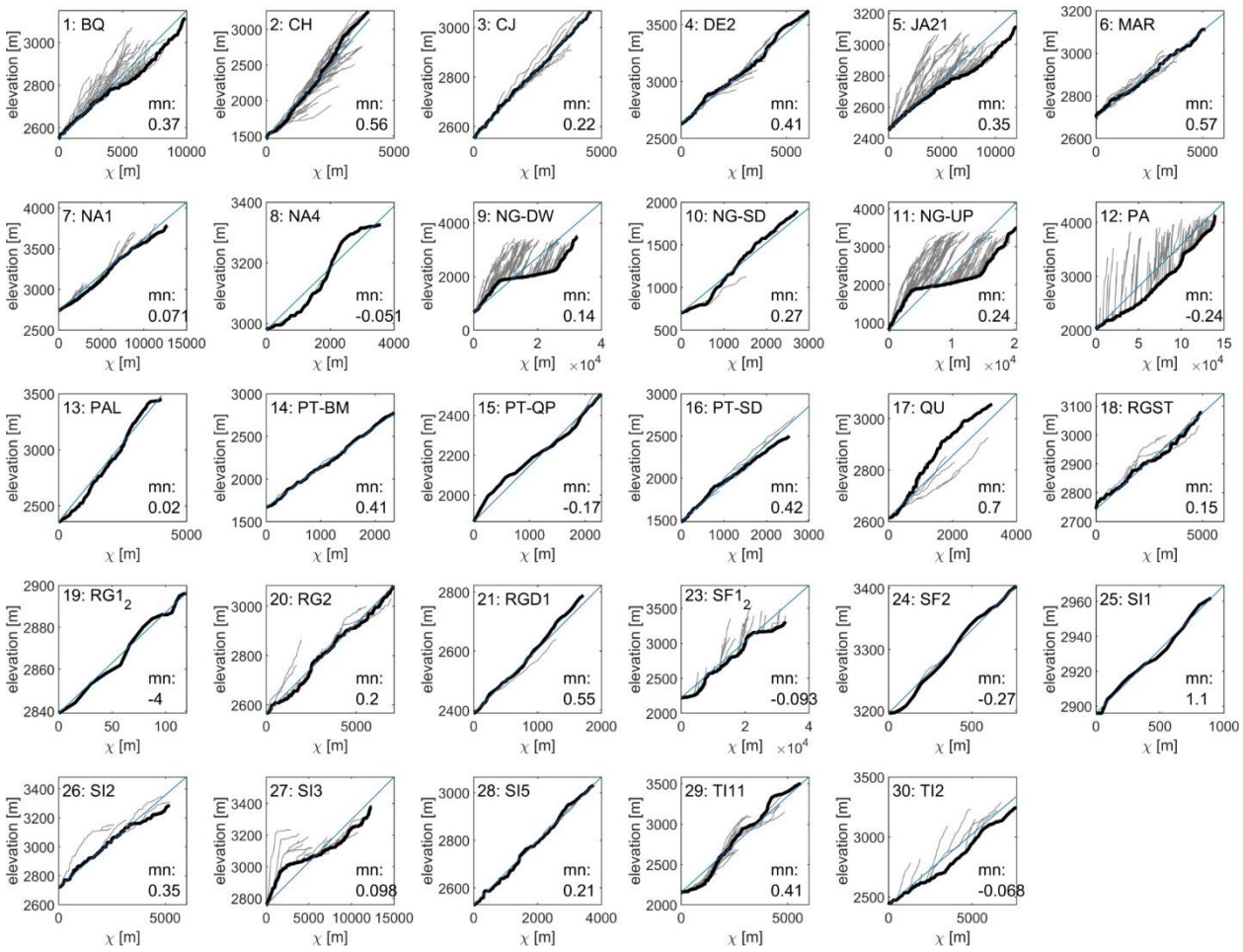

Figure S4: Chi-plots of drainage networks form studied sub-catchments. *mn*-value calculated using the chiplot function in TopoToolbox (Schwanghart and Scherler, 2014), assuming a critical drainage area of 0.5 km².

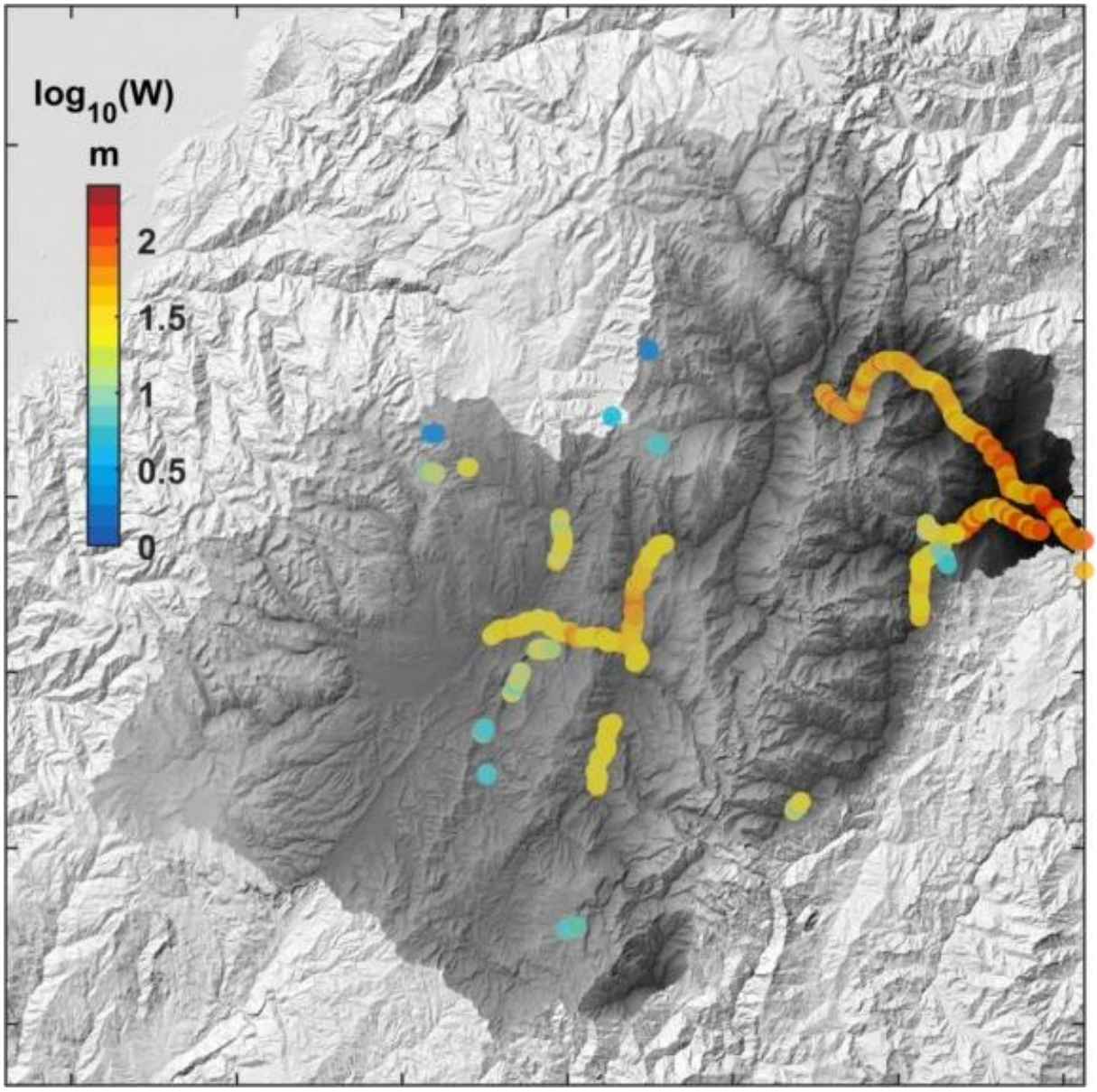

Figure S5: Mapped river width for ca. 120 km of channels overlain on hillshade map based on the 30 m SRTM v3 DEM (NASA JPL, 2013).

References SI

DiBiase, R.A., Whipple, K.X., 2011. The influence of erosion thresholds and runoff variability on the relationships among topography, climate, and erosion rate. J. Geophys. Res. 116, F04036. https://doi.org/10.1029/2011JF002095

DiBiase, R.A., Whipple, K.X., Heimsath, A.M., Ouimet, W.B., 2010. Landscape form and millennial erosion rates in the San Gabriel Mountains, CA. Earth Planet. Sci. Lett. 289, 134–144. https://doi.org/10.1016/j.epsl.2009.10.036

Egüez, A., Gaona, M., Albán., A., 2017. Mapa geológico de la República del Ecuador, Escala 1: 1.000. 000. Quito.

NASA JPL, 2013. NASA Shuttle Radar Topography Mission Global 1 arc second. https://doi.org/10.5067/MEaSUREs/SRTM/SRTMGL1.003

Perron, J.T., Royden, L., 2013. An integral approach to bedrock river profile analysis. Earth Surf. Process. Landforms 38, 570–576. https://doi.org/10.1002/esp.3302

Petersen, M.D., Harmsen, S.C., Jaiswal, K.S., Rukstales, K.S., Luco, N., Haller, K.M., Mueller, C.S., Shumway, A.M., 2018. Seismic Hazard, Risk, and Design for South America. Bull. Seismol. Soc. Am. 108, 781–800. https://doi.org/10.1785/0120170002

Scherler, D., DiBiase, R.A., Fisher, G.B., Avouac, J.-P., 2017. Testing monsoonal controls on bedrock river incision in the Himalaya and Eastern Tibet with a stochastic-threshold stream power model. J. Geophys. Res. Earth Surf. 122, 1389–1429. https://doi.org/10.1002/2016JF004011

Schwanghart, W., Scherler, D., 2014. Short Communication: TopoToolbox 2 - MATLAB-based software for topographic analysis and modeling in Earth surface sciences. Earth Surf. Dyn. 2, 1–7. https://doi.org/10.5194/esurf-2-1-2014

Steinmann, M., Hungerbühler, D., Seward, D., Winkler, W., 1999. Neogene tectonic evolution and exhumation of the southern Ecuadorian Andes: a combined stratigraphy and fission-track approach. Tectonophysics 307, 255–276. https://doi.org/10.1016/S0040-1951(99)00100-6

Vanacker, V., von Blanckenburg, F., Govers, G., Molina, A., Campforts, B., Kubik, P.W., 2015. Transient river response, captured by channel steepness and its concavity. Geomorphology 228, 234–243. https://doi.org/10.1016/j.geomorph.2014.09.013